The mechanism of nanobump formation in femtosecond pulse laser nanostructuring of thin metal films

**Dmitriy S. Ivanov · Baerbel Rethfeld ·
Gerard M. O'Connor · Thomas J. Glynn ·
Alexey N. Volkov · Leonid V. Zhigilei**

Abstract The physical mechanisms responsible for the formation of nanobump structures on a surface of a thin metal film irradiated by a tightly focused femtosecond laser pulse are investigated in a large-scale molecular dynamics simulation. The simulation is performed with a combined atomistic-continuum model adapted for an adequate representation of laser-induced processes at the length-scale of the entire laser spot. The relaxation of the compressive stresses generated by the fast laser heating is identified as the main driving force responsible for the separation of the metal film from the substrate and formation of the nanobump. The kinetics of the transient melting and resolidification, occurring under conditions of the fast cooling due to the two-dimensional electron heat conduction, defines the shape of the nanobump. The predictions of the simulation are related to the surface structures observed in femtosecond laser nanostructuring.

D.S. Ivanov (✉) · B. Rethfeld
Physics Department, Technical University of Kaiserslautern,
Erwin Schroedinger Str. 46, 67663 Kaiserslautern, Germany
e-mail: ivanov@rhrk.uni-kl.de

G.M. O'Connor · T.J. Glynn
National Centre for Laser Applications, Physics Department,
National University of Ireland, Galway, Ireland

A.N. Volkov · L.V. Zhigilei
Department of Materials Science and Engineering, University of
Virginia, 395 McCormick Road, Charlottesville, VA 22904-4745,
USA

1 Introduction

Research efforts towards the development of direct-write laser technologies have yielded a significant progress in fabrication of surface nano- and micro-structures with spatial resolution exceeding the optical diffraction limit. The spatial resolution achievable in laser surface processing is defined by the ability to concentrate the laser energy deposition in a smallest possible domain. Several approaches have been demonstrated to be instrumental in achieving highly localized laser energy deposition, including the use of tightly focused laser beams with the peak laser fluence close to the threshold for material modification [1, 2] or utilization of the optical near field effects, e.g., a local field enhancement in the vicinity of a probe tip [3–6] or a deposited nano/micro-particle [7, 8]. Following the first approach, the direct writing of ordered arrays of hollow bumps and jet-like structures on metal films of different thickness have been recently demonstrated in a number of works [9–12].

While the ability to generate arrays of nanoscale surface features opens up a range of opportunities for practical applications, the processes responsible for the surface nanostructuring are not yet fully understood. Possible mechanisms discussed in literature include Marangoni convection [9], peeling and expansion of the film due to the pressure of evaporating material [11, 12], as well as thermo–elastic and plastic deformation of the film suggested based on recent continuum simulations [13]. Computer modeling of the material response to short pulse laser irradiation indeed has a potential for providing information on the physical processes responsible for the formation of sub-micron frozen surface structures in laser nanotexturing. The fast, highly non-equilibrium character of the laser-induced processes, however, hampers applicability of the continuum models. In particular, it is difficult to describe the phase

transformations and liquid disruption occurring under conditions of strong superheating and high deformation rates within the conventional hydrodynamic computational models.

An attractive alternative to the continuum computational methods is provided by atomistic molecular dynamics (MD) method. While being relatively computationally expensive, MD does not require any assumptions to be made about the processes and mechanisms of interest and is well suited for investigation of fast dynamic material response to short pulse laser irradiation. Calculations performed with a recently developed hybrid atomistic–continuum model [14, 15], have indeed provided microscopic information on the kinetics and mechanisms of laser melting of metal targets [16–19], as well as on the mechanisms of laser spallation [20, 21] and ablation [22]. The ability of large-scale parallel MD simulations to model surface nanostructuring with localized laser energy deposition was recently demonstrated in [23, 24], where a system of more than 200 million atoms interacting via Lennard–Jones potential was used to model the material ejection and crater formation. In this paper we report the results of a large-scale MD simulation aimed at investigation of the processes responsible for laser nanotexturing of metal surfaces. While the immediate goal of this work is to provide insights into the mechanisms responsible for nanobump formation in experiments reported in [9–12], the results of the simulation may also have implications for other laser processing techniques, particularly for surface nanostructuring based on optical near-field effects [3–8].

2 Atomistic–continuum model for surface nanostructuring

The model used in the simulations combines the classical MD method for simulation of non-equilibrium processes of lattice superheating and fast phase transformations with a continuum description of the laser excitation and subsequent relaxation of the conduction band electrons based on the two-temperature model (TTM) [25]. In the combined TTM–MD method, MD substitutes the TTM equation for the lattice temperature, and the diffusion equation for the electron temperature is solved simultaneously with MD integration of the equations of motion of atoms. A complete description of the combined TTM–MD model is given elsewhere [14]. Below we describe the details of the computational setup designed for the simulation of laser nanostructuring of a metal film.

A schematic representation of the computational cell used in the simulation is shown in Fig. 1. The simulations are performed for a 20 nm Ni film deposited on a transparent substrate. The initial MD part of the model is a circular
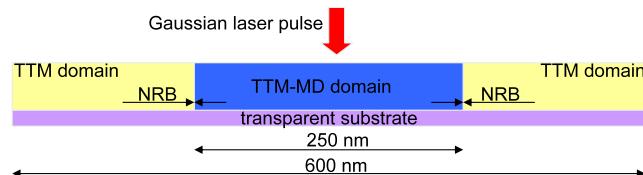

Fig. 1 Schematic representation of the computational setup used in MD–TTM calculations

slab of 250 nm in diameter, where atoms are arranged in the FCC crystal structure with (001) surface oriented parallel to the substrate. The thermal and elastic properties of the Ni film are defined by the interatomic interaction potential, described in this work by the embedded-atom method (EAM) [26]. Some of the parameters of the model EAM Ni material are reported in [14, 20]. The parameters used in the TTM equation for the electron temperature are given in [14]. The top surface of the film, exposed to the laser irradiation, is free to move, whereas the interaction of the bottom side of the film with the substrate is described by Lennard–Jones potential. The parameters of the Lennard–Jones potential are chosen to represent an adhesion of a Ni film to the substrate that is 10 times weaker than the effective strength of Ni–Ni interaction. The substrate is kept rigid during the simulation and the energy exchange between the metal film and the substrate is not allowed. This assumption of the model is justified by the short characteristic time of the processes responsible for the nanobump formation (see Sect. 3) and relatively slow heat exchange between a metal film and a glass substrate.

While the size of the MD part of the combined model is limited to 250 nm in diameter, the TTM equations for the electron and lattice temperatures are solved in a much wider region affected by the thermal conduction, up to more than 300 nm from the center in the radial direction, Fig. 1. A special non-reflective boundary (NRB) condition [27, 28] is applied circumferentially around the MD computational cell. This boundary condition imitates the propagation of the laser-induced radial/circular pressure wave from the MD region to the continuum part of the model and eliminates the artificial effect of the multiple reflections of the wave from the system's radial boundary.

The choice of Ni, rather that Au used in experiments [9–12], is defined by the computational necessity. Strong electron–phonon coupling of Ni (one order of magnitude stronger than that of Au) and negligible contribution of the ballistic energy transport (the range of ballistic electrons in Au is ∼100 nm [29]) result in a fast lattice heating and a high degree of laser energy localization near the laser spot. To quantitatively characterize the extent of spatial energy redistribution during the time of the electron–phonon equilibration, one can consider the effective penetration depth of hot electrons, L_c, introduced in [30]. Following the procedure described in [29–31], the values of L_c can be estimated

to be ~50 nm for Ni and ~700 nm for Au. Thus, the minimum size of the MD region of the model has to be at least 1 µm in size for Au. One can estimate that a circular slab of a gold film with thickness of 20 nm and diameter of 1 µm consists of approximately 10^9 atoms, which is beyond the capabilities of the MD model. For Ni, on the other hand, a 20 nm thick circular slab of 250 nm in diameter provides an adequate description of the laser-induced phase transformations and plastic deformation following a localized laser energy deposition and still contains 85,000,000 atoms, a number that can be treated in a large-scale parallel MD simulation.

Since the sample size is reduced by one order of magnitude, to observe the nanostructuring process similar to [9–12], the diameter of the laser beam in the MD simulation is also reduced by the same order. The simulation is performed with 200 fs laser pulse having Gaussian spatial and temporal profiles and a laser beam diameter (full width at half maximum) equal to 10 nm. Thus, the computational model can be considered to be a scaled down version of the experimental setup used in nanostructuring of Au films. While the difference in the length-scale and material properties does not allow us to establish direct quantitative connections between the computational results and experimental data, the scaled down model can be expected to capture the basic mechanisms responsible for formation of the surface nanostructures.

Note that the TTM–MD simulation involving 85,000,000 atoms interacting by a realistic many-body EAM potential presents a significant computational challenge that can only be addressed with access to advanced computational facilities. The simulation reported in this work is performed with an MPI parallel TTM–MD code optimized for the IBM eServer cluster 1350 recently build at the National Facility at Irish Centre for High End Computing. Using an optimized linked list neighbor search and improved memory consumption, the code has reached a competitive time of ~8 µs spent by a single processor per atom per time step. The simulation was run across 128 processors and required ~1,000 hours of calculations.

3 Results and discussion

The mechanisms of the nanobump formation are investigated in a simulation of a 20 nm Ni film irradiated with a 200 fs laser focused on a 10 nm spot. The average fluence absorbed within the beam diameter (full width at half maximum) is 3.1 J/cm². The visual picture of the laser-induced processes is shown in Fig. 2. In order to provide a clear view of the film separation from the substrate and nanobump formation, only a thin 5 nm slice cut through the center of the MD part of the model is shown in the snapshots taken during the simulation. The atoms in the snapshots are colored according to the local order parameter [14], with blue color indicating the destruction of the original FCC crystalline order due to the fast melting. The melting starts within 2–3 ps after the laser pulse and the radius of the melted region reaches its maximum size of ~32 nm by the time of ~20 ps. The melting process proceeds simultaneously with the separation of the central part of the film from the substrate and generation of a pronounced hollow nanobump due to the rapid bloating of the melted region away from the substrate. Some limited plastic deformation, proceeding mainly by emission of dislocation from the melting front, is observed in a relatively narrow layer adjacent to the melted region.

The insights into the physical mechanisms responsible for the nanobump formation can be obtained by considering the evolution of the electron and lattice temperatures, pressure, and velocity in the direction normal to the substrate. The values of the parameters plotted in Fig. 3 are averaged over a central part of the film with a radius of 2 nm. Due to the small heat capacity of the electrons, the laser excitation results in a large spike of the electron temperature that reaches ~16,000 K by the end of the pulse. The sharp drop of the electron temperature during the first 10 ps of the simulation, Fig. 3(a), is mainly due the fast energy transfer from hot electrons to the lattice. By the time of 12 ps, the electron temperature in the central part of the system drops below the lattice temperature and further decrease of the electron temperature is defined by the two-dimensional electron heat conduction in the radial direction. The fast energy transfer from the electrons to the lattice is also reflected in the initial increase of the lattice temperature, that exceeds the melting temperature of the EAM Ni material, $T_m = 1439$ K [14], at 1 ps after the beginning of the laser pulse and reaches the maximum level of $2.26T_m$ by the time of 15 ps. At later times the heating turns into cooling, with the electron heat conduction and energy transfer from the lattice[1] to the electrons being the dominant cooling mechanisms.

The fast localized heating of the film takes place under conditions of the partial inertial stress confinement [21, 32], when the heating time is shorter than the time needed for the film to expand in response to the thermoelastic stresses. The confinement of the thermoelastic stresses, combined with an additional pressure coming from the suppressed volume expansion associated with the melting process[2], results in the buildup of high, up to 8 GPa, compressive stresses during the first several picoseconds of the simulation, Fig. 3(b) and (d).

---

[1]The use of terms "lattice" and "lattice temperature" in this paper does not imply the preservation of the crystalline order in the system. By using these terms we merely follow the terminology established in the literature presenting TTM calculations.

[2]For the model EAM Ni material, the value of volume change upon melting at zero pressure is found to be $\Delta V_m = 0.46$ cm³/mole and is slightly decreasing with increasing pressure.
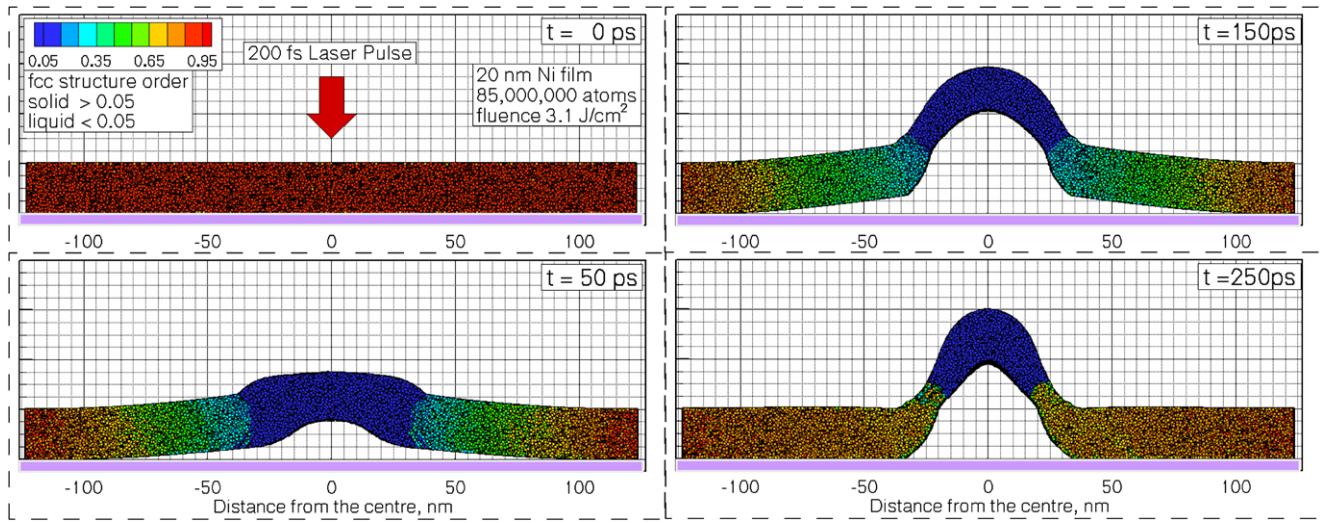
Fig. 2 Snapshots from a TTM–MD simulation of a 20 nm Ni film on a transparent substrate irradiated with a 200 fs laser focused on a 10 nm spot in the middle of the computational cell. The average fluence absorbed within the beam diameter is 3.1 J/cm². Atoms are col- ored according to the local order parameter [14]—red atoms have local crystalline surroundings, blue atoms belong to the liquid and, in the last snapshot, to small crystallites disoriented with respect to the original crystalline structure of the film [33]

The relaxation of the compressive stresses proceeds by expansion in both radial direction and normal to the substrate. In the presence of the rigid substrate, the normal expansion of the film results in the upward acceleration of the film up to a velocity exceeding 300 m/s, Fig. 3(c). The expansion of the film may be described in terms of an unloading wave propagating from the free surface toward the substrate. The reflection of the unloading (tensile) wave from the rigid substrate results in the concentration of the tensile stresses at the film-substrate interface and leads to the separation of the film from the substrate.

An apparent correlation between the time of the film acceleration and the first peak of the compressive pressure, Fig. 3(d), provides clear evidence that the relaxation of the laser-induced compressive stresses generated under conditions of the inertial stress confinement is responsible for the initial acceleration of the central part of the film. Following the initial acceleration, the vertical velocity slowly decreases during the remaining part of the simulation, Fig. 3(c). The decrease of the velocity is related to the resistance of the colder parts of the film to the separation from the substrate. The upward displacement of the central part of the film leads to the elastic deformation of the surrounding areas which relaxes by pooling the film back toward the substrate, Fig. 2. In the melted part of the film, however, the initial momentum induces a hydrodynamic flow of the molten material leading to the formation of a distinct nanobump.

Strong electron temperature gradients established in the radial direction following the initial localized laser energy deposition result in a fast cooling of the electrons and the lattice at later times. At ∼50 ps the lattice temperature at the periphery of the melted region drops below the equilibrium melting temperature, starting a slow process of epitaxial crystallization. At the same time, the fast two-dimensional electron heat conduction continues to cool the melted region, with the lattice temperature in the center of the laser spot dropping down to T_m by 90 ps and down to $0.6T_m$ by the end of the simulation at 250 ps. At such strong undercooling, the slow epitaxial recrystallization gives way to a massive homogeneous nucleation of multiple crystallites within the undercooled liquid region, resulting in a rapid solidification of the nanobump. A detailed analysis of the solidification process producing a nanocrystalline nanobump is presented elsewhere [33].

Relating the results of the simulation to the alternative mechanisms of nanobump formation proposed in the literature, we note that, contrary to the suggestions on the dominant contribution from the pressure of evaporating material [11, 12] or plastic deformation [13], no evaporation or significant plastic deformation of the metal film is observed in the TTM–MD simulation. The area of the nanobump undergoes a transient melting, and the hydrodynamic motion of the melted part of the film prior to the resolidification, rather than plastic deformation [13], is defining the shape of the nanobump. The upward acceleration of the melted film is provided by the relaxation of the initial compressive stresses generated by the fast laser heating, with neither vapor pressure [11, 12] nor Marangoni effect [9] playing a role under the irradiation conditions used in the simulation. The results of the simulation do not exclude, however, the possibility that under different irradiation conditions or for different material system the above mentioned effects may contribute to the generation the surface structures in short pulse laser nanostructuring.
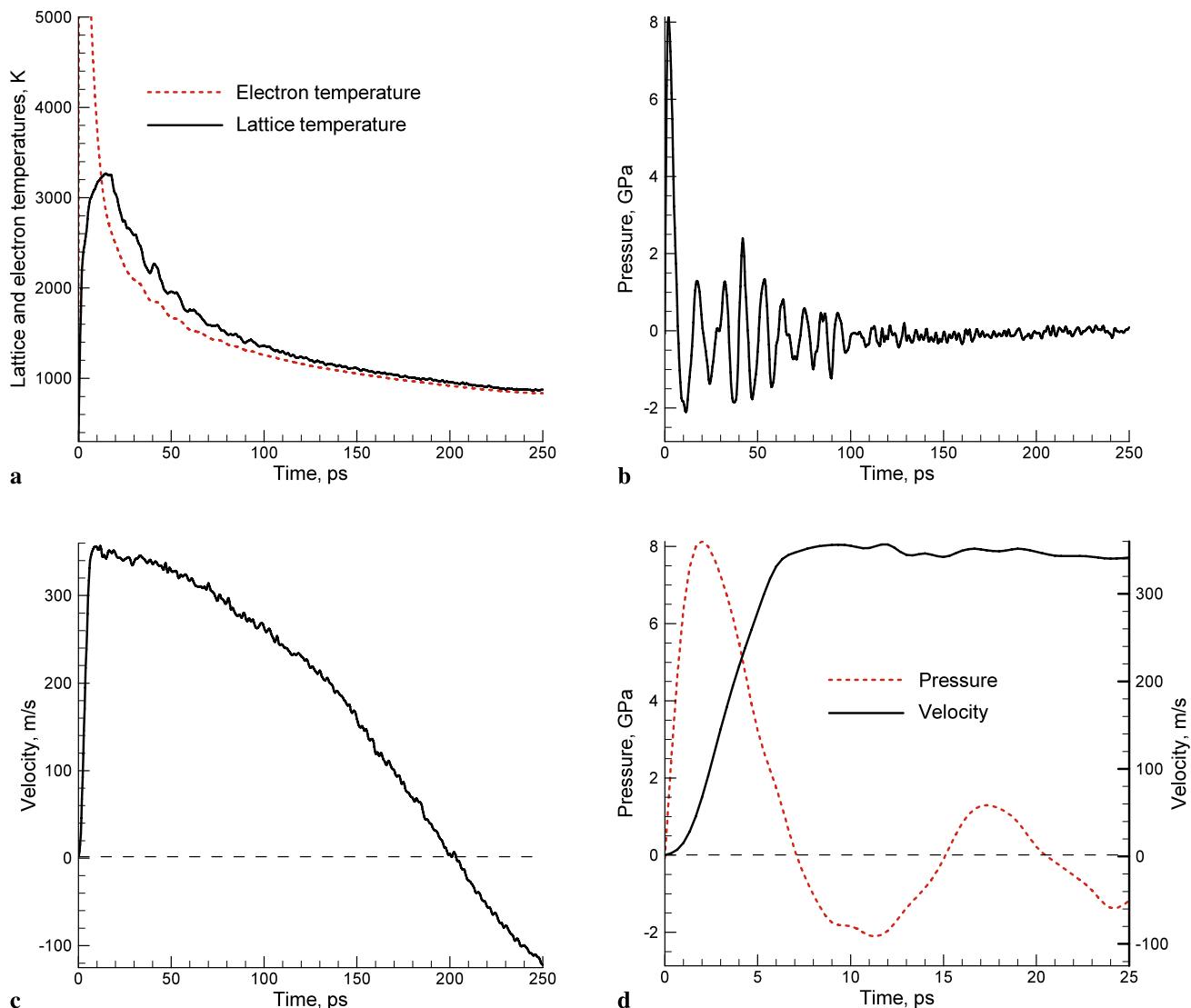
Fig. 3 The time dependences of the electron and lattice temperatures (**a**), pressure (**b**), and velocity in the direction normal to the substrate (**c**) averaged over a part of the film within 2 nm from the center of the laser spot. The initial changes of pressure and velocity during the first 25 ps of the simulation are shown with higher resolution in (**d**)

4 Conclusion

The results of a large scale TTM–MD simulation performed for a thin metal film irradiated by a tightly focused femtosecond laser pulse reveal the physical processes involved in the formation of a nanobump with dimensions comparable to the laser spot. The relaxation of the compressive stresses generated under conditions of the inertial stress confinement is identified as the main driving force responsible for the acceleration of a transiently melted region of the film which results in the bloating of a hollow nanostructure. Two-dimensional electron heat conduction provides the conditions for the fast cooling of the melted region and rapid solidification of a surface feature generated in the process of hydrodynamic motion of the liquid metal. While in the simulation discussed in this work the growth of the nanobump stops at ∼200 ps, one can expect that, at higher excitation levels, the hydrodynamic motion induced by the relaxation of the laser-induced compressive stresses may result in a stronger acceleration and a more active hydrodynamic flow leading to the emergence of jet-like structures that have been observed on top of hollow microbumps in experiments performed at sufficiently high laser fluences.

References

1. P.P. Pronko, S.K. Dutta, J. Squier, J.V. Rudd, D. Du, G. Mourou, Opt. Commun. **114**, 106 (1995)
2. F. Korte, J. Serbin, J. Koch, A. Egbert, C. Fallnich, A. Ostendorf, B.N. Chichkov, Appl. Phys. A **77**, 229 (2003)
3. J. Jersch, F. Demming, J. Hildenhagen, K. Dickmann, Opt. Laser Technol. **29**, 433 (1997)
4. A. Chimmalgi, T.Y. Choi, C.P. Grigoropoulos, K. Komvopoulos, Appl. Phys. Lett. **82**, 1146 (2003)
5. J. Boneberg, H.-J. Münzer, M. Tresp, M. Ochmann, P. Leiderer, Appl. Phys. A **67**, 381 (1998)
6. S.M. Huang, M.H. Hong, Y.F. Lu, B.S. Lukyanchuk, W.D. Song, T.C. Chong, J. Appl. Phys. **91**, 3268 (2002)
7. S.M. Huang, M.H. Hong, B. Lukiyanchuk, T.C. Chong, Appl. Phys. A **77**, 293 (2003)
8. Y. Lu, S.C. Chen, Nanotechnology **14**, 505 (2003)
9. F. Korte, J. Koch, B.N. Chichkov, Appl. Phys. A **79**, 879 (2004)
10. J. Koch, F. Korte, T. Bauer, C. Fallnich, A. Ostendorf, B.N. Chichkov, Appl. Phys. A **81**, 325 (2005)
11. Y. Nakata, T. Okada, M. Maeda, Jpn. J. Appl. Phys. **42**, L1452 (2003)
12. Y. Nakata, N. Miyanaga, T. Okada, Appl. Surf. Sci. **253**, 6555 (2007)
13. Y.P. Meshcheryakov, N.M. Bulgakova, Appl. Phys. A **82**, 363 (2005)
14. D.S. Ivanov, L.V. Zhigilei, Phys. Rev. B **68**, 064114 (2003)
15. C. Schäfer, H.M. Urbassek, L.V. Zhigilei, Phys. Rev. B **66**, 115404 (2002)
16. B. Rethfeld, K. Sokolowski-Tinten, D. von der Linde, S.I. Anisimov, Phys. Rev. B **65**, 092103 (2002)
17. D.S. Ivanov, L.V. Zhigilei, Phys. Rev. Lett. **91**, 105701 (2003)
18. Z. Lin, L.V. Zhigilei, Phys. Rev. B **73**, 184113 (2006)
19. D.S. Ivanov, L.V. Zhigilei, Phys. Rev. Lett. **98**, 195701 (2007)
20. L.V. Zhigilei, D.S. Ivanov, E. Leveugle, B. Sadigh, E.M. Bringa, High-Power Laser Ablation V, Proc. SPIE **5448**, 505 (2004)
21. E. Leveugle, D.S. Ivanov, L.V. Zhigilei, Appl. Phys. A **79**, 1643 (2004)
22. L.V. Zhigilei, Z. Lin, D.S. Ivanov, in *Proceedings of the 2006 ASME International Mechanical Engineering Congress and Exposition (IMECE2006)*, ASME paper IMECE2006-16305 (2006)
23. X.W. Wang, J. Phys. D **38**, 1805 (2005)
24. X.W. Wang, Y.F. Lu, J. Appl. Phys. **98**, 114304 (2005)
25. S.I. Anisimov, B.L. Kapeliovich, T.L. Perel'man, Z. Eksp. Teor. Fiz. **66**, 776 (1974) [Sov. Phys. JETP 39, 375 (1974)]
26. X.W. Zhou, H.N.G. Wadley, R.A. Johnson, D.J. Larson, N. Tabat, A. Cerezo, A.K. Petford-Long, G.D.W. Smith, P.H. Clifton, R.L. Martens, T.F. Kelly, Acta Mater. **49**, 4005 (2001)
27. L.V. Zhigilei, B.J. Garrison, Mat. Res. Soc. Symp. Proc. **538**, 491 (1999)
28. C. Schafer, H.M. Urbassek, L.V. Zhigilei, B.J. Garrison, Comput. Mater. Sci. **24**, 421 (2002)
29. J. Hohlfeld, S.-S. Wellershoff, J. Gudde, U. Conrad, V. Jahnke, E. Matthias, Chem. Phys. **251**, 237 (2000)
30. P.B. Corkum, F. Brunel, N.K. Sherman, T. Srinivasan-Rao, Phys. Rev. Lett. **61**, 2886 (1988)
31. D.S. Ivanov, L.V. Zhigilei, Appl. Phys. A **79**, 977 (2004)
32. L.V. Zhigilei, B.J. Garrison, J. Appl. Phys. **88**, 1281 (2000)
33. D.S. Ivanov, B. Rethfeld, G.M. O'Connor, T.J. Glynn, Z. Lin, L.V. Zhigilei, in preparation